Materials Horizons

ROYAL SOCIETY OF CHEMISTRY

REVIEW

View Article Online
View Journal | View Issue

Cite this: *Mater. Horiz.*, 2023, **10**, 1990

Nucleophilic deposition behavior of metal anodes†

Yuqian Li,[ab] Jie Shu [a] and Liyuan Zhang *[a]

Nucleophilic materials play important roles in the deposition behavior of high-energy-density metal batteries (Li, Na, K, Zn, and Ca), while the principle and determination method of nucleophilicity are lacking. In this review, we summarize the metal extraction/deposition process to find out the mechanism of nucleophilic deposition behavior. The key points of the most critical nucleophilic behavior were found by combining the potential change, thermodynamic analysis, and active metal deposition behavior. On this basis, the inductivity and affinity of the material have been determined by Gibbs free energy directly. Thus, the inducibility of most materials has been classified: (a) induced nuclei can reduce the overpotential of active metals; (b) not all materials can induce active metal deposition; (c) the induced reaction is not changeless. Based on these results, the influencing factors (temperature, mass, phase state, induced reaction product, and alloying reactions) were also taken into account during the choice of inducers for active metal deposition. Finally, the critical issues, challenges, and perspectives for further development of high-utilization metal electrodes were considered comprehensively.

Received 17th February 2023,
Accepted 28th March 2023

DOI: 10.1039/d3mh00235g

rsc.li/materials-horizons

1. Introduction

Although lithium-ion batteries have achieved great success in commercialization, metal batteries (Li, Na, K, Zn, and Ca) are considered to be next generation high-performance batteries due to their high energy density. For the high proportion of active substances and low redox potential of the metal anode, the two future development directions of high-energy-density batteries include high-utilization-metal batteries and anode-free metal batteries.[1–4] However, the application of metal electrodes encounters restrictions on dendrite growth. These dendrites consume active materials and aggravate battery-side reactions, which leads to the loss of substances. These will restrict the preparation and application of high utilization rate metal anodes and even no metal anode, which causes a huge obstacle to the realization of high energy density metal batteries.[5–11]

A metal anode with a high utilization rate or even no extra metal means a large amount of metal participates in extraction/deposition, which indicates that the current collector cannot maintain a complex structure.[12–14] Therefore, the affinity between the current collector and the active metal will directly determine the stability of the electrode structure. Some structures, like the root structure of a tooth,[15] and the root structure of a tree,[16] are very useful for constructing stable fluid-collecting electrode structures. Nevertheless, electrodes with poor affinity are easy to form and grow active metals on the surface of the metal, resulting in problems such as the formation of dendrites and dead metals.

To improve the affinity of the interface, metal derivatives are routinely used as the induction core to induce reactivity. Various compounds are applied as inducers to build stable metal anodes,[17–20] such as oxides,[21–38] nitrides,[39–48] fluorides,[49–54] and phosphides.[55–61] These compounds can improve the affinity of the interface and help form high-utilization-metal batteries. Nevertheless, the mechanism of nucleation, cycling of metal electrodes, and the determination of ions' behavior are blurry. Moreover, only one suitable induction material is considered and analyzed as the induction core, and the systematization and regularity are lacking. For example, most of the derivatives have a certain degree of inductivity in Li metal electrodes, while which one material is the most suitable is unclear; the derivatives that can be used in other metal batteries (Na, K, Zn, Mg, and Al) are unidentified, and whether all the derivatives are available for inducing the deposition of metal is uncertain. As a result, the selection and application of metal inducers still lack a complete selection system. It is of vital importance to construct a system with no need for complicated experimentation and that can directly judge the inducibility of a substance.

[a] School of Materials Science and Chemical Engineering, Ningbo University, Ningbo 315211, China. E-mail: zhangliyuan@nbu.edu.cn
[b] School of Energy and Power Engineering, Nanjing University of Science and Technology, Nanjing, 210094, China

† Electronic supplementary information (ESI) available. See DOI: https://doi.org/10.1039/d3mh00235g

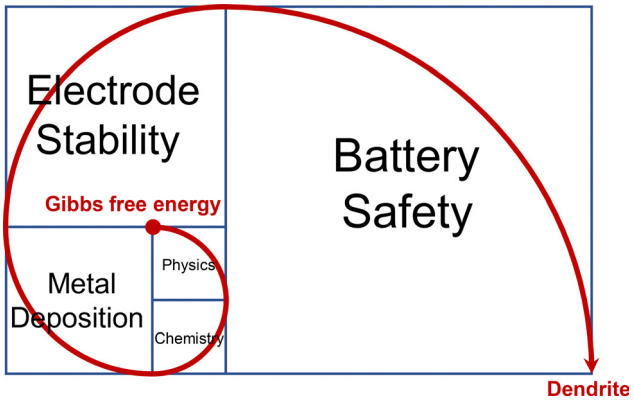

Fig. 1 Illustration of deposition behavior of metal anodes: the basic physical chemistry determines the rules, which ultimately affect the safety of the battery.

In this review, we summarized and analyzed the affinity between metals and current collectors, which help to realize a high-utilization metal electrode and high-energy density metal batteries (Fig. 1). First, the deposition potential, substance, and energy change in the metal dissolution/deposition process are analyzed and Gibbs free energy is considered as an important basis for judging. Then according to the existing literature and articles, the reaction-free energy is systematically reviewed, summarized, classified, and calculated to find out the relevant change trend and the judicial law of the inducing material. After that, the reaction states of the battery under different working conditions and other interference factors such as temperature and reaction products are explored to identify whether the reaction law is eternal.

2. Discussion

2.1. Deposition reaction in metal batteries

To answer the question of whether the substance is inducible in the deposition process, the battery reaction mechanism needs to be clarified. Usually, metals are deposited on the substrate material to form metal anodes. The energy undulation and influencing factors like overpotential are analyzed specifically and quantitatively.[62–64] The energy undulation in the initial stage includes the change of Gibbs free energy, and the change of Gibbs free energy leads to the material variety and the difference of reaction energy barriers. Taking Li batteries as an example, Li becomes Li^+ on the anode side and then deposits on Li foil on the cathode side as shown in Fig. 2a. The reaction at the anode side is shown by Li metal atoms crossing the energy barrier ($\Delta G_{bar.,Li\rightarrow Li^+}$) to an excited state with exoteric additional energy and losing electrons resulting in an oxidized state of Li^+. This procedure needs extra energy ($\Delta G_{bar.,Li\rightarrow Li^+}$) and releases energy ($\Delta G_{bar.,Li\rightarrow Li^+} + \Delta G_{Li\rightarrow Li^+}$) after crossing the barrier. The reactive ion reaction (eqn (1)) is shown below:

$$Li\text{–}e^- = Li^+ \quad \Delta G_{Li\rightarrow Li^+} = -293.3\ kJ\ mol^{-1} \qquad (1)$$

Though the conversion of Li to Li^+ is a spontaneous reaction, there is an energy barrier that needs to be overcome. When the deposition current density increases, with the increasing number of Li turning to Li^+, the energy required to activate the Li atoms is also enlarged as the number of Li atoms participating in the above reaction proportionally increases. Since the reactions are identical, the energy changes of the initial deposition and the stable deposition are the same as the reaction continues.

When it comes to the cathode, there is another situation. There are various cathodes, such as Cu foil, carbon, and carbon doped with compounds, which are used as substrates of Li. In a stable deposition process, as there is already a layer of lithium on the cathode surface, the substrate hardly affects the deposition process. Thus, nucleation energy is not required and Li^+ will cross another energy barrier ($\Delta G_{bar.,Li}$) to an active state and be reduced to Li[65] (eqn (2)).

$$Li^+ + e^- = Li \quad \Delta G_{Li^+\rightarrow Li} = 293.3\ kJ\ mol^{-1}\ (blue\ line) \qquad (2)$$

During the reduction of Li^+, $\Delta G_{bar.,Li}$ is needed to cross the barrier and extra energy $\Delta G_{bar.,Li\rightarrow Li^+}$ (293.3 kJ mol^{-1}) will be released. Taking all these processes, the system releases energy ($\Delta G_{Li\rightarrow Li^+}$) at the anode and absorb energy ($\Delta G_{Li^+\rightarrow Li}$) at the cathode (blue line), which means the reaction reaches an energy balance.

However, the first cycle of the battery (original deposition) is inconsistent and two different situations depend on the substrates (eqn (3)).

$$Li^+ + e^- = \frac{x}{2y}M + \frac{1}{2}Li_2O - \frac{1}{2y}M_xO_y \qquad (3)$$

Reaction A: $\Delta G > 293.3\ kJ\ mol^{-1}$ (yellow line)

Reaction B: $\Delta G < 293.3\ kJ\ mol^{-1}$ (red line)

Due to different reactions, the energy barriers are changed as the yellow and red lines shown in Fig. 2a. Productions have different Gibbs free energies, so the lithophilic substrate ($\Delta G > 293.3\ kJ\ mol^{-1}$) needs less energy ($\Delta G_{bar.,B\rightarrow Li^+}$) than that of a stable deposition while lithium-phobic substrate ($\Delta G < 293.3\ kJ\ mol^{-1}$) needs extra energy ($\Delta G_{bar.,A\rightarrow Li^+}$).

The difference between the initial deposition and the stable deposition is reflected in the voltage. Specific quantitative relationships between energy and voltage including Gibbs free energy and other factors are analyzed as follows. Fig. 2b shows the half battery structure and overpotential curves of different substrate materials. Correspondingly, the yellow and red lines refer to the electrode reactions of $\Delta G > 293.3\ kJ\ mol^{-1}$ and $\Delta G < 293.3\ kJ\ mol^{-1}$; the blue line refers to the Cu or other non-reactive substrates.

Due to the huge amount of unstable factors in the initial deposition stage, the equilibrium state is analyzed first to reduce the influencing factors. Voltage is proportional to energy (eqn (4)):

$$\Delta G = -nEF \qquad (4)$$

According to this relationship, the ion reaction (Li, Na, K, and other metals) potential can be calculated (ESI†).

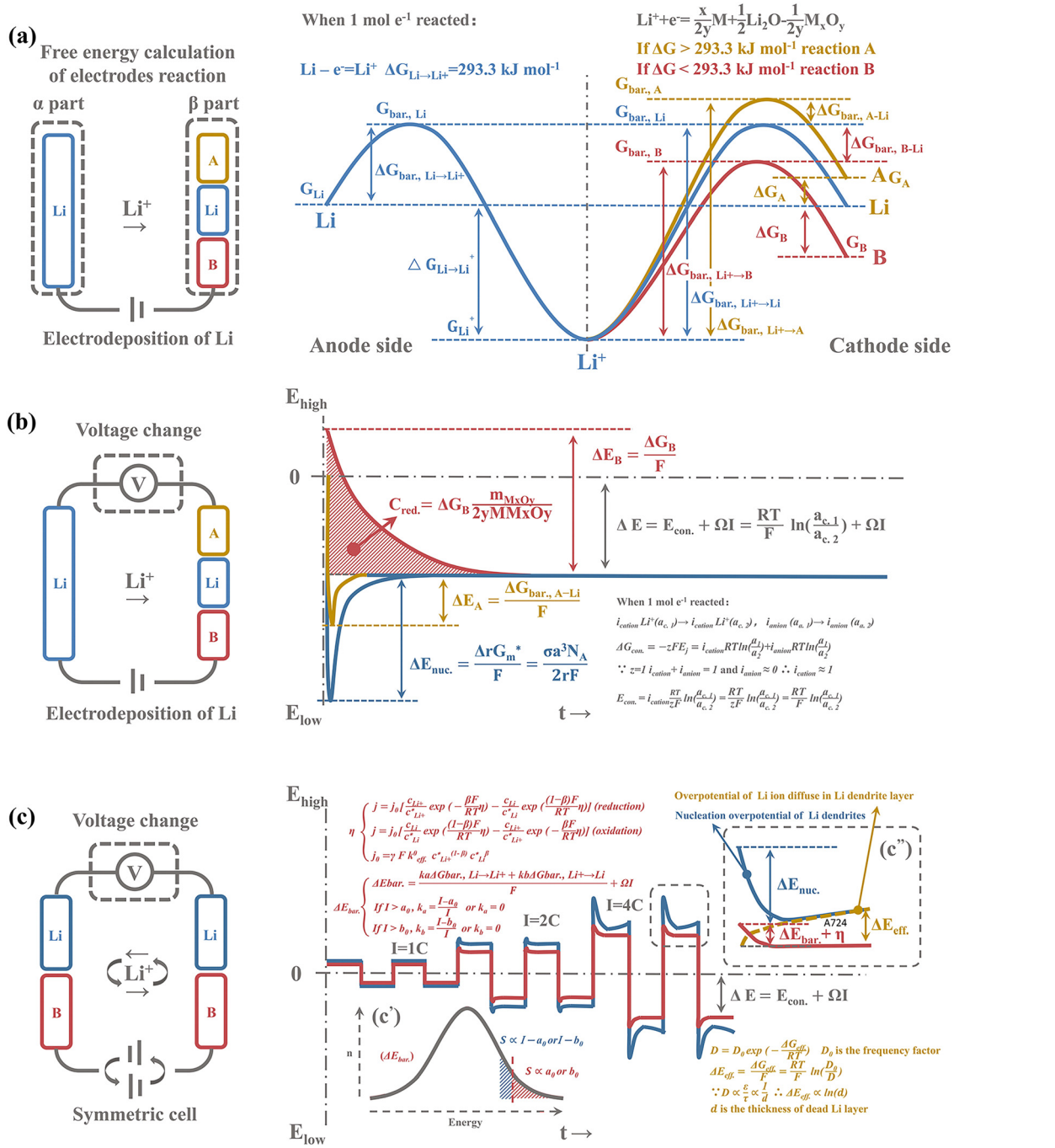

Fig. 2 Deposition reaction in metal batteries. (a) Gibbs free energy change curve of Li^+ in the initial dissolution–deposition process. (b) The components of over-potential in the initial stage of Li^+ deposition. (c) Overpotential transformation of symmetric batteries during cycling.

Theoretically, if the energy released at the anode can be used to excite the cathode reaction completely with no energy loss, it needs no extra energy to prompt the reaction. While voltage is the reflection of energy, the overpotential should be zero. However, this is not the case. It can be found that the energy needed by electrical equipment, and the migration from the anode to the cathode of Li ions form concentration potential, and the inevitable resistance of the electrolyte causes energy loss. Specifically, the overpotential ΔE is the sum of concentration and resistance for the tested battery according to the Nernst equation and Ohm's law (eqn (5)):

$$\Delta E = E_{con.} + \Omega I \quad (5)$$

That means resistance for the battery is directly related to overpotential as the partial potential of the internal resistance is the product of resistance and current, which means the higher the deposition current density, the greater the over-potential and equilibrium deposition potential are.

$E_{con.}$ can be calculated as follows:

when 1 mol e^- reacted, $z = 1$, $i_{cation}Li^+(a_{c.1}) \rightarrow i_{cation}Li^+(a_{c.2})$, $i_{anion}(a_{a.1}) \rightarrow i_{anion}(a_{a.2})$

$$E_{con.} = -zFE_j = i_{cation}RT\ln\left(\frac{a_{c.1}}{a_{c.2}}\right) + i_{anion}RT\ln\left(\frac{a_{c.1}}{a_{c.2}}\right) \quad (6)$$

due to $i_{cation} + i_{anion} = 1$ and $i_{anion} \approx 0$, $i_{cation} \approx 1$

$$E_{con.} = i_{cation}\frac{RT}{zF}\ln\left(\frac{a_{c.1}}{a_{c.2}}\right) = \frac{RT}{zF}\ln\left(\frac{a_{c.1}}{a_{c.2}}\right) = \frac{RT}{F}\ln\left(\frac{a_{c.1}}{a_{c.2}}\right) \quad (7)$$

$$\Delta E = \frac{RT}{F}\ln\left(\frac{a_{c.1}}{a_{c.2}}\right) + \Omega I. \quad (8)$$

After derivation of eqn (6) and (7), it can be concluded that the partial potential of the concentration is dependent on temperature; the higher the temperature, the greater the partial potential when ion activity is consistent. In short, the controlling factors of the overpotential in the stable deposition state are identified: the deposition current density, current, resistance, temperature and Li^+ concentration are positively correlated with overpotential. Experimental verification with controlling current density variables is shown in Fig. S1 (ESI†); for the same ion deposition on the same substrate, the overpotential increases with the increasing current density. The experimental results in all three representative metals (Li, Na, and K) are consistent with the speculative results which can confirm the correctness of the theory.

The initial sedimentation reaction is discussed as follows. The Cu substrate does not react with Li^+ and is not a lithophilic material. As electrons travel much faster than ions, when Li atoms in the anode are oxidized to Li^+, the corresponding electrons are transferred more quickly to the positive electrode. After that, the Li^+ in the electrolyte is reverted to a Li metal synchronously on Cu foil and thus the first solution-deposition process is completed. The energies required for these two steps are $\Delta G_{bar.,Li\rightarrow Li^+}$ and $\Delta G_{bar.,Li}$, respectively. As the energies during deposition and extraction are offset, the generally extra energy input is necessary due to the concentration difference and resistance ($E_{con.} + \Omega I$). Additional nucleation energy is needed for the Cu substrate.

Moreover, due to the poor contact affinity between Cu and Li metal, extra nucleation energy is needed.[66] Compared with the stable deposition process and initial sedimentation reaction, the energy required increases.

$$\Delta E_{nuc.} = \frac{\Delta_r G^*_m}{F} = \frac{16\pi\sigma^3 {T_m}^3}{3{L_m}^2\Delta TF} \quad (9)$$

Thus, for the same current density, the inducer plays an important role in the overpotential. Cu substrates,[67–69] which possess poor contact affinity with the Li metal, need the nucleation energy $\Delta E_{nuc.}$ and are predicted to have the maximum initial deposition overpotential. However, if the substrate is an inducer with Li, the $\Delta E_{nuc.}$ can be smaller or even offset which means a smaller overpotential.[70–72] The experimental proof is further shown in Fig. S2 (ESI†). For the K metal half-cell, the discharge process gives rise to the formation of K carbides on carbon electrodes and the following deposition process can display the overpotential value. Hard carbon shows the highest K capacity, which means the highest K carbide containment. As a result, hard carbon after discharging shows the lowest overpotential.

Additionally, both lithium-phobic and lithophilic substrates are combined with carbon to guarantee conductivity normally, so there is no nucleation energy. For the lithium-phobic substrate (A), the energy needed is the sum of $\Delta G_{bar.,Li\rightarrow Li^+}$ and $\Delta G_{bar.,A\rightarrow Li}$, which is greater than the stable deposition energy $\Delta G_{bar.,Li\rightarrow Li^+}$. In other words, the initial overpotential is the combination of stable overpotential ΔE and the voltage formed by the extra energy barrier ΔE_A (eqn 10):

$$\Delta E_A = \frac{\Delta G_{bar.\,A-Li}}{F} \quad (10)$$

If lithophilic inducer B is chosen, the initial deposition can be easier. Using the same analysis method, the reduced voltage change compared with the equilibrium sedimentation process can be expressed as eqn (11):

$$\Delta E_B = \frac{\Delta G_{bar.\,B-Li}}{F} \quad (11)$$

Moreover, the reduced energy and the stable deposition energy can be calculated by comparing eqn (7) and (8). If 1 mol Li^+ reacts, the energy difference is ΔG_B. When the mass of the inducer reacted is $M_{M_xO_y}$, the integral of the area between two overpotential curves is displayed in eqn (12):

$$C_{red.} = \Delta G_B\frac{m_{M_xO_y}}{2yM_{M_xO_y}} \quad (12)$$

Up to now, an overall understanding of the energy changes during metal deposition is built and a quantitative equation of the overpotential based on Gibbs free energy and energy barrier is established.

The overpotential of symmetric batteries is determined by complex influencing factors, including current density, cycling time, the diffusion of ions, and the ion reaction (Fig. 2c). For the pure K electrode under normal current density (lower than the current density that leads to sand's time), the stable deposition mainly refers to the barrier of activation energy of reaction η (eqn (13)–(15)).

$$j = j_0\left[\frac{c_{Li^+}}{c^*_{Li^+}}\exp\left(-\frac{\beta F}{RT}\eta\right) - \frac{c_{Li}}{c^*_{Li}}\exp\left(\frac{(1-\beta)F}{RT}\eta\right)\right]\text{(reduction)} \quad (13)$$

$$j = j_0\left[\frac{c_{Li}}{c^*_{Li}}\exp\left(\frac{(1-\beta)F}{RT}\eta\right) - \frac{c_{Li^+}}{c^*_{Li^+}}\exp\left(-\frac{\beta F}{RT}\eta\right)\right]\text{(oxidation)} \quad (14)$$

$$j_0 = \gamma F k^0_{eff.}{c^*_{Li^+}}^{(1-\beta)}{c^*_{Li}}^{\beta}. \quad (15)$$

The sharp peak of overpotential at the beginning of deposition is due to the nucleation of Li. Along with the cycling time, the overpotential is much larger due to the inevitable formation of dendrites. Subsequently, Li^+ diffusion in the dead Li layer is more difficult. Increased diffusion resistance leads to an

enlarged overpotential in the following deposition which can be specifically expressed as:

$$\Delta E_{\text{eff.}} = \frac{\Delta G_{\text{eff.}}}{F} = \frac{RT}{F}\ln\left(\frac{D_0}{D}\right) \quad (16)$$

For the deposition on the electrode with an inducer, which can inhibit the formation of dendrites, there is no nucleation overpotential due to the affinity of nucleated sites and no diffusion overpotential without the dendrite layer. Additionally, it is worth noting that beside the nucleation overpotential, there are also overpotentials caused by metal deposition and growth, ion diffusion and migration, and ion diffusion in the dendrite layer formed in the later stage.[73] Therefore, the disappearance of the nucleation overpotential cannot be seen in the initial deposition, while the reduction in the sum overpotential can be detected. Moreover, the stable growth process in the later stage leads to a constant potential, namely the equilibrium overpotential of eliminating nucleation overpotential. Theoretically, the slight increase in the overpotential of the induced electrode is due to the reaction barrier of the ion reaction. As displayed in Fig. 2c′, the energy of Li^+ conforms to normal distribution, the number of active ions with enough energy to cross the reaction energy barrier is proportional to the current density, and the other white area in Fig. 2c′ represents the number of ions that need extra energy to cross the barrier.

This section focuses on the battery reaction mechanism: (1) a lithophilic substrate needs less energy while a lithiumphobic substrate needs more energy. (2) The controlling factors of the overpotential in the stable deposition state are identified: operating current density and resistance, temperature and Li^+ concentration. (3) In the initial stage of battery deposition, Li nucleation results in a large overpotential; the diffusion of Li^+ in the dead Li layer leads to the increase of overpotential in the subsequent deposition reaction.

2.2. Inducers reducing the initial overpotential

From eqn (3)–(6), the controlling factor of the overpotential includes intrinsic battery factors (battery internal resistance) and working condition factors. As shown in Fig. S3 (ESI†), the substrate largely determines the electrochemical deposition behavior. Inducers play an important role in enhancing alkali metal nucleation sites. The introduction of nucleation sites builds a robust substrate to form a tightly bound structure with alkali metals. In the case of ensuring the working state of the battery, the way to reduce the overpotential is to change the affinity and reaction energy of the substrate. Through the theoretical analysis and experimental verification of the deposition process, Gibbs free energy theory was introduced to explain this process. In addition, this method can determine whether a substance can act as an inducer or not.

Different oxides of different elements are analyzed to determine if a substance can be used as an inducer. The reaction of the sedimentary state should be clear: the reaction of the anode in a half battery is the same:

$$A = A^+ + e^- \quad A = (Li, Na, K)\ \Delta G_{A10} \quad (17)$$

Table 1 The inductivity of common oxides in alkali metal batteries

Mass	M_xO_y	$\Delta G_{M_xO_y}$	ΔG_{Li12}	ΔG_{Na12}	ΔG_{K12}	Calc.
107.87	Ag_2O	−11.18	−275.46	−183.95	−155.79	115.87
26.98	Al_2O_3	−1582.27	−17.34	74.17	102.33	16.99
74.92	As_2O_5	−782.09	−202.84	−111.34	−83.17	22.98
137.33	BaO	−525.35	−18.38	73.13	101.29	76.67
9.01	BeO	−579.06	8.48	99.99	128.15	12.51
40.07	CaO	−603.51	20.70	112.21	140.37	28.04
140.12	CeO_2	−1025.38	−24.71	66.80	94.96	43.03
58.93	CoO	−214.20	−173.95	−82.45	−54.28	37.47
58.93	Co_3O_4	−794.90	−181.69	−90.18	−62.02	30.10
52.00	CrO_2	−544.90	−144.83	−53.32	−25.16	21.00
52.00	Cr_2O_3	−1058.07	−104.71	−13.20	14.96	25.33
132.91	Cs_2O	−308.41	−126.85	−35.34	−7.18	140.91
63.55	CuO	−128.29	−216.91	−125.40	−97.24	39.78
63.55	Cu_2O	−147.88	−207.11	−115.61	−87.44	71.55
55.85	FeO	−251.44	−155.33	−63.82	−35.66	35.93
55.85	Fe_2O_3	−742.29	−157.34	−65.83	−37.67	26.62
55.85	Fe_3O_4	−1015.23	−154.15	−62.64	−34.48	28.94
69.72	Ga_2O_3	−998.34	−114.66	−23.16	5.01	31.24
72.63	GeO	−237.20	−162.45	−70.95	−42.78	44.32
72.63	GeO_2	−521.31	−150.73	−59.22	−31.06	26.16
200.59	HgO	−58.53	−251.79	−160.28	−132.12	108.30
24.30	MgO	−568.94	3.42	94.93	123.09	20.15
54.94	MnO	−362.90	−99.60	−8.10	20.07	35.47
54.94	MnO_2	−465.14	−164.77	−73.26	−45.10	21.74
54.94	Mn_3O_4	−1283.23	−120.65	−29.14	−0.98	28.60
95.95	MoO_2	−533.05	−147.79	−56.28	−28.12	31.99
92.91	Nb_2O_5	−1765.86	−104.47	−12.96	15.20	26.58
58.69	NiO	−211.54	−175.28	−83.78	−55.61	37.35
207.21	PbO	−188.65	−186.73	−95.22	−67.06	111.61
207.21	PbO_2	−215.40	−227.20	−135.70	−107.53	59.80
44.96	Sc_2O_3	−1819.37	22.18	113.68	141.85	22.99
78.97	SeO_2	−171.47	−238.18	−146.68	−118.52	27.74
118.71	SnO	−256.77	−152.67	−61.16	−33.00	67.36
118.71	SnO_2	−520.00	−151.05	−59.55	−31.38	37.68
87.62	SrO	−561.40	−0.35	91.16	119.32	51.81
47.87	TiO_2	−889.41	−58.70	32.81	60.97	19.97
50.94	V_2O_5	−1419.54	−139.10	−47.59	−19.43	18.19
183.84	WO_2	−533.86	−147.59	−56.08	−27.92	53.96
65.38	ZnO	−320.48	−120.81	−29.31	−1.15	40.69
91.22	ZrO_2	−1339.72	53.88	145.39	173.55	30.81

The values of ΔG_{A10} depend on the type of metal, such as ΔG_{Li10}, ΔG_{Na10}, and ΔG_{K10} are −293.3 kJ mol^{-1}, −261.9 kJ mol^{-1}, and −283.3 kJ mol^{-1}, respectively.[74–77] However, the reaction of the cathode is different. As oxide is one of the most widely used type of inducer, it is chosen and discussed. For example, the reactions on several common bases are listed below:

Carbon or Cu substrate:

$$A = A^+ + e^- \quad A = (Li, Na, K)\ \Delta G_{A11'} \quad (18)$$

Oxides-doped carbon:

$$1/(2y)M_xO_y + A^+ + e^- = x/(2y)M + 1/2A_2O \quad A = (Li, Na, K)\ \Delta G_{A11'} \quad (19)$$

If $\Delta G_{A11'}$ is smaller than ΔG_{A11}, the oxide can be an inducer for active metal deposition. These two equations are subtracted to compare more conveniently:

$$1/(2y)M_xO_y + A = x/(2y)M + 1/2A_2O \quad (A = Li, Na, K)\ \Delta G_{A12} \quad (20)$$

$$\Delta G_{A11'} - \Delta G_{A11} = \Delta G_{A12}$$

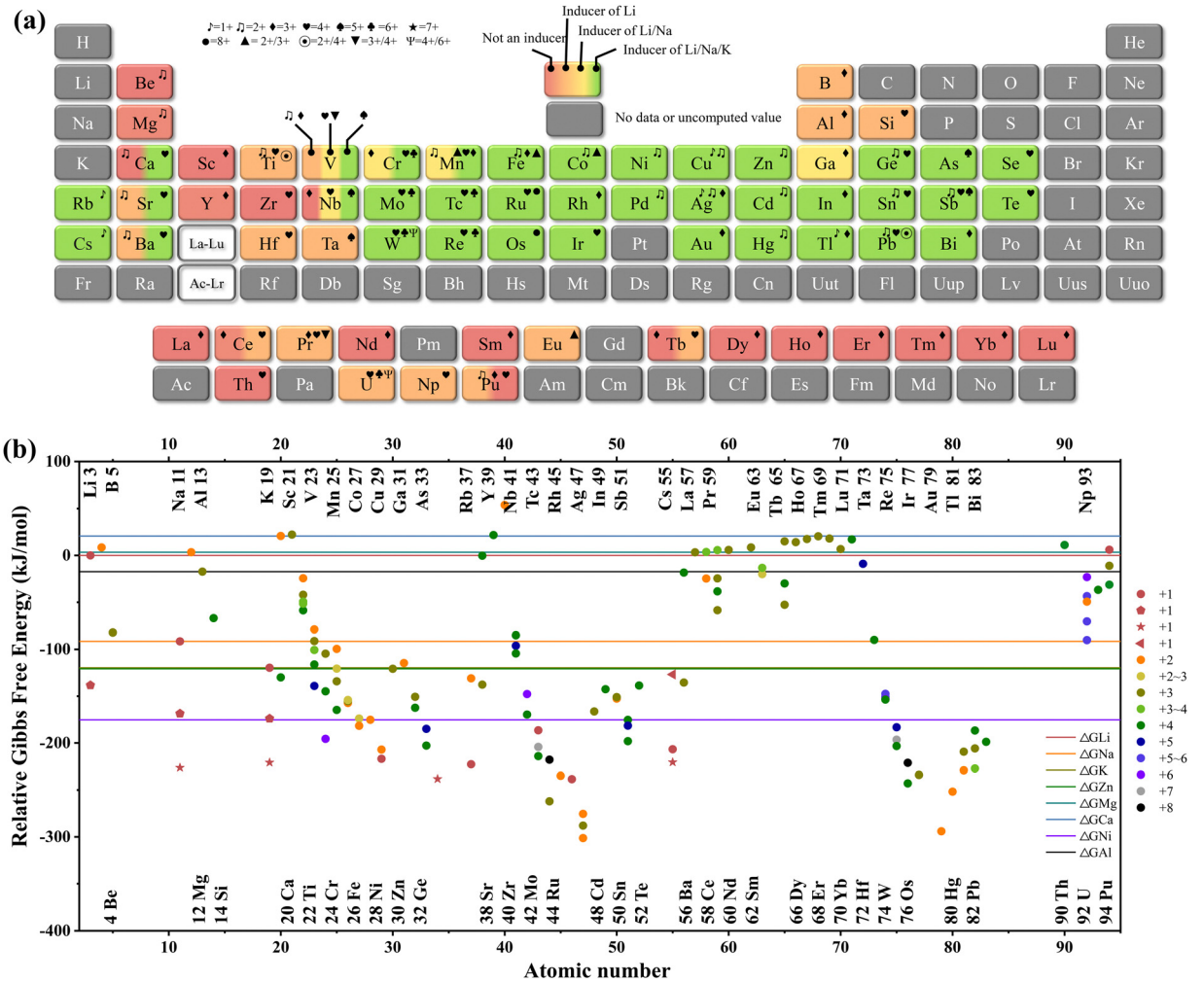

Fig. 3 Oxides' inducer to reduce the initial overpotential. (a) The inductivity of different oxides arranged in the periodic table in Li, Na and K metal batteries. (b) Inductive summary of typical oxides in common metal electrodes.

If $\Delta G_{A12} < 0$, the oxide can be an inducer. The smaller the ΔG_{A12} ($\Delta G_{A11'}$), the better the inductivity. Table 1 lists the inductivity of common oxides in alkali metal (Li, Na, and K) batteries. Additionally, the inductivity of the other metal batteries mentioned in the scientific work (Zn, Mg, Ca, Ni, and Al) are shown in the ESI.†[65,78–80]

As $\Delta G_{A12} = 1/2G_{f,A_2O} - 1/(2y)\Delta G_{f,M_xO_y}$, if the active metal of the batteries is fixed, the $G_{f,\ A_2O}$ is fixed. Thus, ΔG_{A12} depends on the value of $\Delta G_{f,M_xO_y}$, and y. The harder the formation of the oxide, the better the inductivity of the energy. Fig. 3 exhibits the inductivity of different oxides in Li, Na, and K metal batteries to show the tendency clearly. Ignoring the measurement error of forming Gibbs free energy and special properties of special elements, it can be concluded as follows. For elements in the same main family, there is a tendency that the inductivity enhances with the increase of atomic number. Generally, reducibility reduces with the increasing atomic number (same main family). Similarly, for elements in the same period, there is a tendency that the inductivity enhances with the increase in atomic number.

Actually, for the same oxide, due to the $\Delta G_{A12} = 1/2G_{f,A_2O} - 1/(2y)\Delta G_{f,M_xO_y}$, the difference of ΔG_{A12} depends on the $G_{f,A2O}$. As shown in Fig. 3b, the Gibbs free energy difference between different oxides in K and Na batteries is constant. Noticeably, the metal valence in oxides, nitride, and fluoride does not affect the calculation, and the related data are shown in the ESI† and Fig. S4.

Besides the inducibility of the oxide being confirmed, another determinant of the selection of the inducer is the relative atomic mass of the inducer. The most prominent advantage of metal batteries is their high energy density. Therefore, as an inactive substance of the battery, the inducer also needs to take its quality into account when considering it. The mass of oxides needed to react 1 mol e^- of 8 normal metal batteries is calculated *via* the reaction equation and the molar mass of the substance. Integrating the inducibility with mass (Fig. 4, Fig. S5, ESI† and Table 1) can guide the selection of oxide, fluorides, and nitrides inducers.[81–89] The stuff on the bottom left has less mass and more inductivity. For better differentiation, colors are used to indicate selection trends.

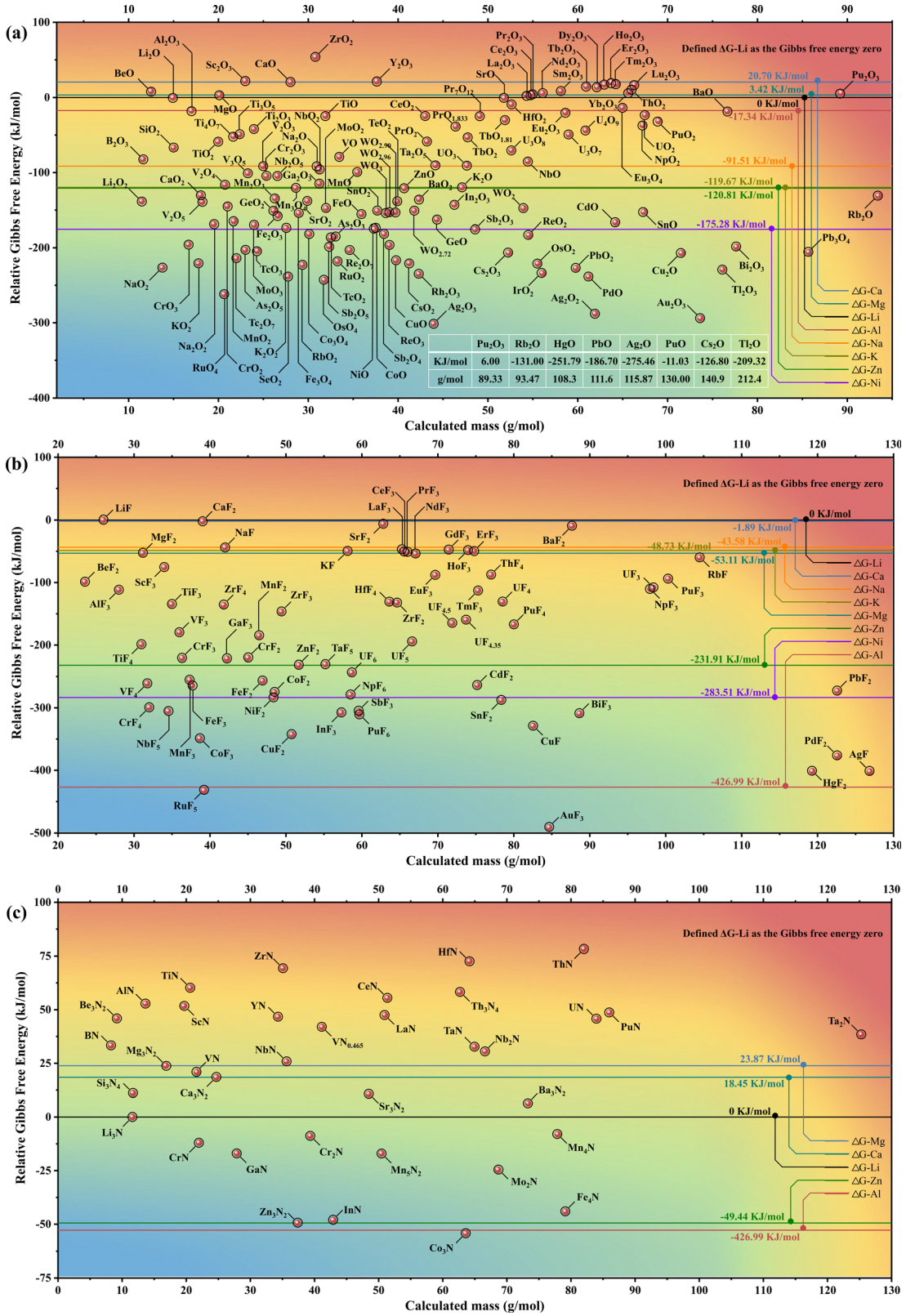

Fig. 4 Inductivity of different substances considering mass factors. The selection of (a) oxide, (b) fluoride and (c) nitride inducers integrated the inducibility with the mass of common metal batteries synthetically.

The cooler the hue, the more we need. Oxides like NaO_2 and Cr_2O_3 not only have small relative atomic masses but also can induce the deposition process, while Pu_2O_3 can do just the opposite.

According to the calculation results, MgO is not a suitable inducer for Li, Na, or K. To further indicate the correctness and rationality of the judgment rule, the MgO inducer is applied (Fig. S6–S8, ESI†). Fig. S6a and b (ESI†) show the morphology of carbon-loaded MgO particles (MgO@C). Fig. S6c (ESI†) indicates the uniform elemental distribution and Fig. S6d (ESI†) displays the MgO characteristic peaks. Fig. S7 (ESI†) reveals the overpotential of carbon with/without MgO. MgO has little effect on Li deposition potential while it can increase Na and K deposition overpotentials with no side effects for stable deposition. This is due to the ignorable Gibbs free energy change compared with pure carbon electrodes. These results verified the negative impact of MgO during the process of deposition. Moreover, Co_3O_4 composite carbon materials are also used to deposit Na^+, and the positive effect, just as we predicted, is successfully manifested (Fig. S8, ESI†).[90,91]

The inducibility of the other compounds is also calculated systematically in the same way.[78,79,92] Table 2 puts the metal compounds together for intuitive comparison. It can be concluded generally that fluorides show the strongest inductance, oxides come next, while nitrides show the smallest inductance for the same metal. Regardless of the preparation problem, fluorides can be an appropriate choice to reduce the overpotential and produce dendrite-free electrodes. It should be noted that when nitride reacts with Na and K, the products are not stable (decomposing into N_2), so the nitride inducer is not suitable for Na and K electrodes.[93–97]

In this part, the inductance of materials is analyzed systematically based on the deposition mechanism: (1) the inductivity increases with increasing atomic number for elements in the same main family and period. (2) Fluorides show the strongest inductance, oxides come next, while nitrides show the smallest inductance for the same metal. (3) Besides the inducibility of the oxide being confirmed, another determinant of the selection of the inducer is the relative atomic mass of the inducer.

2.3. Inductivity of different substances at the non-room temperature

The above results refer to the Gibbs change of the reaction at room temperature. Actually, in the course of practical experiments and applications, molten metals mixed with certain base materials become an important way to modify the metal electrodes and improve the stability of metal batteries. Nevertheless, combining the metal with substrates is difficult and the binding force is weak. Thus, substances such as oxides are used to promote the reaction and enhance the adhesion. Oxide is taken as an example to discuss the relationship. The reaction is consistent with the sum of the cathode and anode reactions in the deposition process.

$$1/(2y)M_xO_y + A = x/(2y)M + 1/2A_2O \quad (A = Li, Na, K)\ \Delta G_{A12} \tag{21}$$

Therefore, the basic data are still available in the table.

Notably, the inductivity in melting temperature is not the same as that at room temperature because the Gibbs free

Table 2 The comparison of the inductivity of oxides, fluorides, nitrides, and phosphides in Li batteries

M_xO_y	ΔG_{Li12}	ΔG_{Li11}	M_xF_y	ΔG_{Li12}	ΔG_{Li11}	M_xN_y	ΔG_{Li12}	ΔG_{Li11}	M_xP_y	ΔG_{Li12}	ΔG_{Li11}
1	Oxides	Oxides	2	Fluorides	Fluorides	3	Nitrides	Nitrides	4	Phosphide	Phosphide
Al_2O_3	275.96	−17.34	AlF_3	181.67	−111.63	AlN	346.08	52.78	AlP	264.87	−28.43
Au_2O_3	−0.73	−294.03	AuF_3	−197.76	−491.06						
BaO	274.92	−18.38	BaF_2	283.85	−9.45	Ba_3N_2	299.69	6.39			
BeO	301.78	8.48	BeF_2	194.33	−98.97	Be_3N_2	339.23	45.93			
CaO	314.00	20.70	CaF_2	291.41	−1.89	Ca_3N_2	311.75	18.45			
Ce_2O_3	296.90	3.60	CeF_3	241.93	−51.37	CeN	348.74	55.44			
CoO	119.35	−173.95	CoF_2	17.92	−275.38				CoP	258.99	−34.31
Cr_2O_3	188.59	−104.71	CrF_3	72.45	−220.85	CrN	281.32	−11.98			
Cs_2O	166.45	−126.85	CsF	230.02	−63.29						
Cu_2O	86.19	−207.11	CuF	−35.82	−329.12				Cu_3P	230.74	−62.56
CuO	76.39	−216.91	CuF_2	−49.54	−342.84						
FeO	137.97	−155.33	FeF_2	36.23	−257.07						
Fe_2O_3	135.96	−157.34	FeF_3	28.74	−264.56						
Ga_2O_3	178.64	−114.66	GaF_3	71.51	−221.79	GaN	276.33	−16.97	GaP	242.69	−50.61
In_2O_3	150.69	−142.61	InF_3	−14.63	−307.93	InN	245.19	−48.11	InP	237.93	−55.37
La_2O_3	296.58	3.28	LaF_3	245.90	−47.40	LaN	340.76	47.46			
MgO	296.72	3.42	MgF_2	240.19	−53.11	Mg_3N_2	317.17	23.87			
Mn_2O_3	159.10	−134.20	MnF_3	37.91	−255.39	MnN	249.13	−44.17	MnP	249.13	−44.17
Nd_2O_3	299.09	5.79	NdF_3	239.17	−54.13						
NiO	118.02	−175.28	NiF_2	9.79	−283.51						
PbO	106.57	−186.73	PbF_2	20.08	−273.22						
Pu_2O_3	299.33	6.03	PuF_3	199.25	−94.05	PuN	341.96	48.66			
Sb_2O_3	117.97	−175.33	SbF_3	−12.32	−305.62						
Sc_2O_3	315.48	22.18	ScF_3	217.85	−75.45	ScN	345.01	51.71			
SrO	292.95	−0.35	SrF_2	286.91	−6.39	Sr_3N_2	303.93	10.63			
ThO_2	304.44	11.14	ThF_4	205.53	−87.77	Th_3N_4	351.50	58.20	ThP	325.96	32.66
Ti_2O_3	251.22	−42.08	TiF_3	158.59	−134.71	TiN	353.47	60.17			
V_2O_3	202.09	−91.21	VF_3	113.53	−179.77	VN	314.11	20.81			
ZnO	172.49	−120.81	ZnF_2	61.39	−231.91	Zn_3N_2	243.86	−49.44	Zn_3P_2	226.04	−67.26

energy of the matter is not a constant. Ignoring the electrolyte, it can be drawn from the previous conclusion that in general, the higher the temperature, the better the inductivity is. Nevertheless, the inductivity of the substance is dynamically changed at different temperatures surely.

The change of Gibbs free energy at high temperatures is analyzed. To acquire the calculated results, the Gibbs free energy of different substances and the Gibbs free energy change of several reactions are considered. For the pure metal ion reaction, the calculation is as follows:

$$Li^+ + e^- = Li\ \Delta G_{T,Li^+\rightarrow Li} \quad (22)$$

$\Delta G_{T,Li^+\rightarrow Li}$ is the Gibbs free energy change in this reaction. The value of $\Delta G_{Li^+\rightarrow Li}$ in the low-temperature range (solid without a phase change) is known. To extend the temperature range and express the $\Delta G_{T,Li^+\rightarrow Li}$ more accurately, the equation for G_{Li^+} is calculated. The standard voltage value of the propylene glycol solvent is taken as an example (eqn (23)).

$$E_{T,Li^+\rightarrow Li} = -3.48 - (T - 298.15) \times 850 \times 10^{-6} \text{ (at phase transition temperature)}$$

$$\Delta G_{T,Li^+\rightarrow Li} = zE_{T,Li^+\rightarrow Li} \times F$$

$$= \left[-3.48 - (T - 298.15) \times 850 \times 10^{-6}\right] \times 96\,485.3328$$

$$= -0.0560T + 352.4539 \text{ (accurate data in the ESI†)} \quad (23)$$

Through existing data of $G_{T,Li}$, the value of $G_{T,Li}$ is fitted into two parts, solid and liquid. The equation of G_{T,Li^+} at phase transition temperature is calculated based on the data of $G_{T,Li}$ changing with temperature. As G is a state function, the variation trend of G_{T,Li^+} is assumed to be consistent above the phase transition temperature.[98] $\Delta G_{T,Li^+\rightarrow Li}$ above the phase transition temperature can be obtained by G_{Li} (fitted) and G_{T,Li^+} (calculated).

$$\Delta_r H_m^{\Theta}(T) = \Delta H_0 + \Delta aT + \frac{1}{2}\Delta bT^2 + \frac{1}{3}\Delta cT^3 \quad (24)$$

$$\Delta_r S_m^{\Theta}(T) = \Delta a + IR + \Delta a \ln T + \Delta bT + \frac{1}{2}\Delta cT^2 \quad (25)$$

$$\Delta_r G_m^{\Theta}(T) = \Delta H_0 - IRT - \Delta aT \ln T - \frac{1}{2}\Delta bT^2 - \frac{1}{6}\Delta cT^3 \quad (26)$$

$$\Delta a = \sum_B \nu_B a_B \quad \Delta b = \sum_B \nu_B b_B \quad \Delta c = \sum_B \nu_B c_B \quad (27)$$

$\Delta_r G_m^{\Theta}$ increases with the increase of the temperature, because Δa, Δb, and Δc are positive values. Moreover, the Gibbs

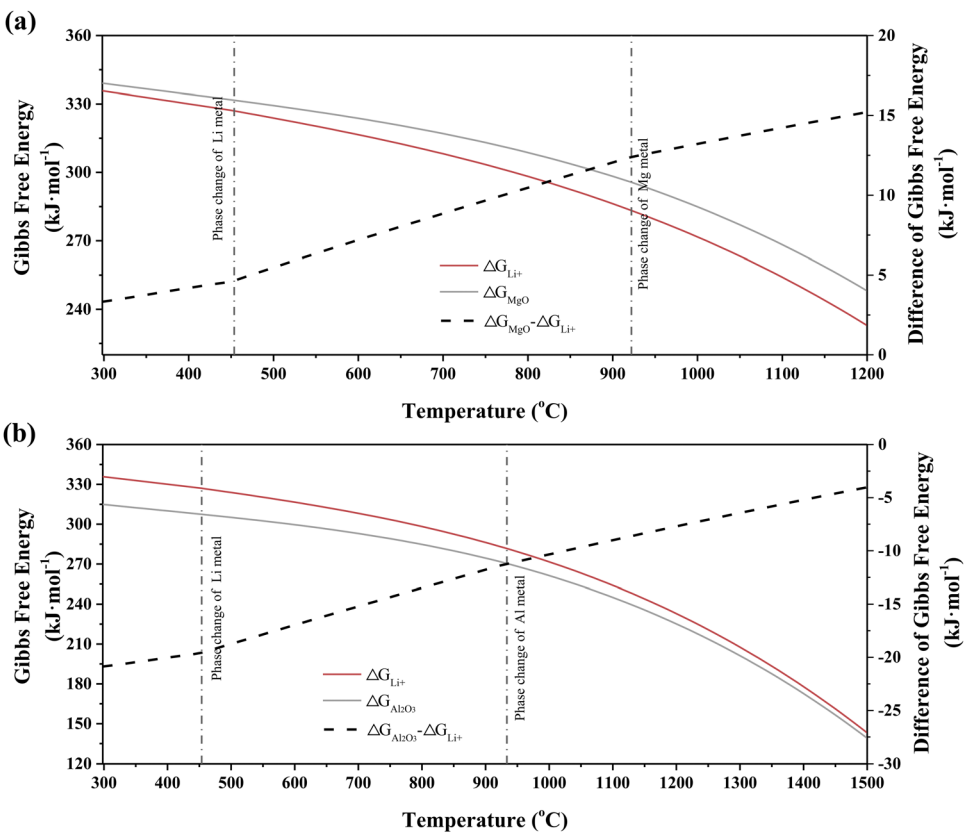

Fig. 5 Inductivity at the non-room temperature. (a) Inductivity of MgO in Li metal batteries at different temperatures. (b) Inductivity of Al_2O_3 in K metal batteries at different temperatures.

free energy of oxides can be obtained from the following method:

$$xM + \frac{y}{2}O_2 = M_xO_y \quad \Delta G_{M_xO_y} = G_{M_xO_y} - xG_M - \frac{y}{2}G_{O_2} \quad (28)$$

$\Delta G_{M_xO_y}$ is easy to be calculated by fitting the standard Gibbs free energy of oxides. Nevertheless, it is hard to find the reason for the change of its value in essence. Hence, $\Delta G_{M_xO_y}$ is obtained by fitting the standard Gibbs free energy of M metal, O_2, and M_xO_y. To make the simulation more accurate, the phase transition temperature is used as the boundary to separate different parts for fitting.

At last, the temperature coefficients of $\Delta G_{T,M_xO_y}$ and $\Delta G_{T,Li+}$ are determined. The Gibbs free energy-temperature trend is shown in Fig. 5. More importantly, the inductivity of different temperatures is calculated. Fig. 5a and b illustrate the inductivity of MgO and Al_2O_3 at temperatures from 300 to 1500 K. With the increase in temperature, the effect of oxides on lithium also varies. Normally, the inductiveness is enhanced in most cases. There are two turning points in the $\Delta G_{T,M_xO_y-Li+}$. As the trend of G_{T,O_2} is fixed, these two turning points are the results of the shifting trends of M and Li. The G, H trend alters with the phase change, which corresponds to the turning points shown in Fig. 5. It may be complicated to model the trend of $\Delta G_{T,M_xO_y-A^+}$ through the G of the reaction. Simulating the ΔG of M_xO_y and active ions' (Li^+ *etc.*) changes directly can get the approximate results (Fig. S9, ESI†).

This part analyzes the inductance of substances at non-room temperature. The affinity of the same substance varies with temperature and the tendency of the inductivity of different substances varies with temperature. Furthermore, the data availability of the phase transition process is questionable.

2.4. Alloying reaction

Regardless of the reaction of the inducer at room temperature or other temperatures,[99,100] the metallicity of elements in the inducer will be reduced to simple metals (such as Ag), some of which will undergo an alloying reaction (such as Li–Ag alloy) with the active metal. Whether or not the alloying reaction occurs, the formation of solid solutions and intermetallic compounds after the alloying reaction depends on the reduced metallic element and the type of anode of the metal battery.[101–104]

As shown in Fig. 6a–c, the alloying reaction with different metals is distinguished for the Ag-contained inducer. Li and Ag exist in different alloyed forms and the phase change temperature is relatively low, which means the alloying reaction between these two metals is easy. However, there is no alloy between Li and K around room temperature as the diagram shows, which means that there is no alloying reaction between them. Only when the temperature increases above 1000 °C or the system has a stronger energy, a weak alloying reaction can occur. The properties of Na are between Li and K as Na can alloy with Ag, but this reaction is more difficult than that of Li. Furthermore, Fig. 6d exhibits the alloying reaction between different elements with three alkali metals Li, Na, and K. The alloying ability of alkali metals can be obtained easily

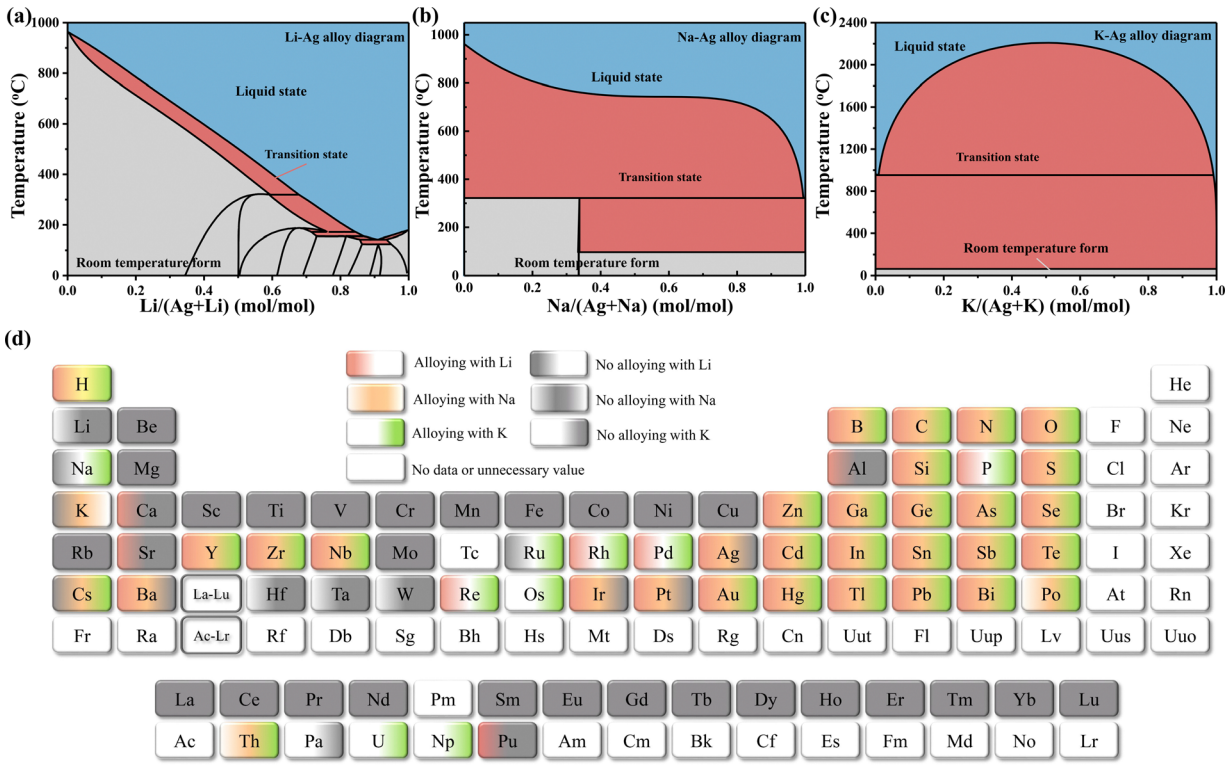

Fig. 6 Inductivity at the non-room temperature. (a) Li–Ag, (b) Na–Ag, and (c) K–Ag binary alloy phase diagram. (d) Alloying reaction between different elements with Li, Na, and K.

and the alloying characteristics of the three metals have no obvious rule.

This section mainly elaborates on the form of the product after the induction reaction. There is an alloying reaction between various elements and active metal electrodes; it has a great impact on the reaction product and the state after the reaction; whether the alloying is beneficial needs further research.

This section mainly describes the products after the induction reaction. A variety of elements can undergo alloying reactions with active metal electrodes; whether the alloying reaction occurs or not has a great impact on the state after the reaction product. In this regard, whether alloying is beneficial needs further research.

3. Conclusions and prospects

The design and use of batteries with high energy density and high utilization rate of active substances put forward severe requirements for the design of metal batteries, especially the alkali metal electrodes. To achieve high stability and high utilization of metal electrodes as far as possible, it is of great significance to rationally use inducers to construct stable structures, avoid dendrite growth, and improve the activity ratio. By analyzing and summarizing the current data and auxiliary deposition experiments, we can draw the following conclusions.

(1) Rational use of induced nuclei has a certain positive effect based on electrochemical reaction analysis. The presence of inducible nuclei can induce the material to react and deposit at specific sites rather than grow directly on the current collector surface. Gibbs free energy can be used to determine whether the deposition reaction is preferred for the active metal reaction or induced nuclear reaction. When choosing high-utilization metal batteries, especially anode-free batteries, the size and molar mass of inducible materials should be considered. For example, inducible materials should be like seeds which have relatively light weight and buried deep in a soil-like current collector, as roots like active metals grow from the seeds to the surface and form dense, smooth metals eventually. Our previous work did a similar demonstration. This staggered structure is the key to achieving a uniform electric field of the electrode.[15] Thus, the traditional metal-based current collector needs surface treatment or coating of a carbon layer to achieve this goal. Specifically, some metals formed by a displacement reaction can alloy with active metals. However, more research needs to be done to identify whether alloys are advantageous. During the working process, stripping the active metal might lead to the structural collapse of the monolithic alloy, such as the Li–Ag alloy.

(2) Not all materials can induce active metal deposition. First of all, if the Gibbs free energy to induce a material to react with an active metal is greater than the deposition free energy of the active metal, a large overpotential will be generated which is not inducible and the active metal tends to grow on the surface of the active metal. Moreover, lithium metal-inducible materials may not be suitable for other metals. For example, the induced reaction products of nitrides in Na and K electrodes are azides (NaN_3 and KN_3), and nitrides cannot exist stably.

(3) Many factors affect the induced reaction, especially the temperature. For materials that are not induced near room temperature, increasing the temperature may achieve an induced reaction. Therefore, it is necessary to choose materials with stronger inductivity rather than the inductivity close to the inductivity decision line (*i.e.* not strong inductivity). Furthermore, if heating causes a phase transition of the active metal (solid to liquid phase), the Gibbs free energy parameter is going to change dramatically, which has a very large effect on the induced reaction. The phase transition process is considered in this article, but the applicability of the data after the phase transition is lacking. Some data are relatively old and need to be further updated.

Based on the above analysis and discussion, here are some suggestions for the construction of high-energy-density metal batteries. First, 100% utilization of active metals (anode-free battery) is not the most urgent problem to solve at the moment. It is more feasible to gradually increase the utilization rate of metals and choose cheaper materials. Furthermore, more strategies such as the construction of an alloy structure, 3D structure substrate, and the compound of nucleophilic materials and metals can also be of advantages.

Second, the distribution of induced nuclei is very important. At present, only carbon materials can achieve the induced behavior which is similar to the rooting effect of active metals. In the future, traditional current collectors may be able to achieve this goal through partial alloying. Finally, the choice of an electrolyte with better fluidity and wettability is necessarily critical. It would be advantageous to apply a high wetting electrolyte to form a stable electrode and then achieve a stable deposition and dissolution interface of the active metal. Nevertheless, this process is currently very cumbersome, so the use of metal batteries is still not that easy.

This article systematically discusses and summarizes the previous research results and data on the metal battery deposition reaction-induced nucleation, puts forward the relevant judgment basis, and carries out the necessary experimental verification. This can provide theoretical support for the exploration and development of the preparation technology based on the high utilization rate of metal electrodes in the future, and it is expected to play a more important role in the production and application of batteries in the later stage.

Author contributions

Conceptualization, data curation, formal analysis, investigation, methodology, project administration, resources, supervision, validation, and visualization: Y. Q. Li and L. Y. Zhang; software and roles/writing – original draft: Y. Q. Li; writing – review & editing and funding acquisition: L. Y. Zhang and J. Shu.

Conflicts of interest

There are no conflicts to declare.

Acknowledgements

This work was supported by the National Natural Science Foundation of China (51901205), the Natural Science Foundation of Zhejiang Province (LY21E010003), and the College Leading Talents Training Program of Zhejiang Province.

References

1 W. Liu, P. Liu and D. Mitlin, *Chem. Soc. Rev.*, 2020, **49**, 7284–7300.
2 R. Sanderson, *Chemical bonds and bonds energy*, Elsevier, 2012.
3 Z. Yang, W. Liu, Q. Chen, X. Wang, W. Zhang, Q. Zhang, J. Zuo, Y. Yao, X. Gu and K. Si, *Adv. Mater.*, 2023, DOI: **10.1002/adma.202210130**.
4 X. Yu, Y. He, J. Sun, K. Tang, H. Li, L. Chen and X. Huang, *Electrochem. Commun.*, 2009, **11**, 791–794.
5 P. Cao, X. Zhou, A. Wei, Q. Meng, H. Ye, W. Liu, J. Tang and J. Yang, *Adv. Funct. Mater.*, 2021, **31**, 2100398.
6 H. Liu, J. G. Wang, W. Hua, H. Sun, Y. Huyan, S. Tian, Z. Hou, J. Yang, C. Wei and F. Kang, *Adv. Sci.*, 2021, **8**, 2102612.
7 X. Han, H. Leng, Y. Qi, P. Yang, J. Qiu, B. Zheng, J. Wu, S. Li and F. Huo, *Chem. Eng. J.*, 2022, **431**, 133931.
8 Y. An, Y. Tian, Q. Man, H. Shen, C. Liu, Y. Qian, S. Xiong, J. Feng and Y. Qian, *ACS Nano*, 2022, **16**, 6755–6770.
9 Z. Yang, C. Lv, W. Li, T. Wu, Q. Zhang, Y. Tang, M. Shao and H. Wang, *Small*, 2021, **18**, 2104148.
10 J. Zheng, Z. Cao, F. Ming, H. Liang, Z. Qi, W. Liu, C. Xia, C. Chen, L. Cavallo and Z. Wang, *ACS Energy Lett.*, 2021, **7**, 197–203.
11 D. Wang, D. Lv, H. Peng, N. Wang, H. Liu, J. Yang and Y. Qian, *Nano Lett.*, 2022, **22**, 1750–1758.
12 S. Lang, M. Colletta, M. R. Krumov, J. Seok, L. F. Kourkoutis, R. Wen and H. D. Abruña, *Proc. Natl. Acad. Sci. U. S. A.*, 2023, **120**, e2220419120.
13 S. Li, H. Zhu, Y. Liu, Z. Han, L. Peng, S. Li, C. Yu, S. Cheng and J. Xie, *Nat. Commun.*, 2022, **13**, 4911.
14 Y. Zhong, S. Zhou, Q. He and A. Pan, *Energy Storage Mater.*, 2022, **45**, 48–73.
15 Y. Li, L. Zhang, S. Liu, X. Wang, D. Xie, X. Xia, C. Gu and J. Tu, *Nano Energy*, 2019, **62**, 367–375.
16 X. Tang, D. Zhou, P. Li, X. Guo, B. Sun, H. Liu, K. Yan, Y. Gogotsi and G. Wang, *Adv. Mater.*, 2020, **32**, 1906739.
17 N. Lu, C. Shao, X. Li, F. Miao, K. Wang and Y. Liu, *Ceram. Int.*, 2016, **42**, 11285–11293.
18 X. Wang, Y. Liu, Y. Wang and L. Jiao, *Small*, 2016, **12**, 4865–4872.
19 F. Klein, B. Jache, A. Bhide and P. Adelhelm, *Phys. Chem. Chem. Phys.*, 2013, **15**, 15876–15887.
20 D.-H. Liu, Z. Bai, M. Li, A. Yu, D. Luo, W. Liu, L. Yang, J. Lu, K. Amine and Z. Chen, *Chem. Soc. Rev.*, 2020, **49**, 5407–5445.
21 W. Chen, R. V. Salvatierra, M. Ren, J. Chen, M. G. Stanford and J. M. Tour, *Adv. Mater.*, 2020, **32**, 2002850.
22 J. Y. Kim, O. B. Chae, G. Kim, W. B. Jung, S. Choi, D. Y. Kim, S. Moon, J. Suk, Y. Kang and M. Wu, *Energy Environ. Mater.*, 2022, DOI: **10.1002/eem1002.12392**.
23 Y. Mei, J. Zhou, Y. Hao, X. Hu, J. Lin, Y. Huang, L. Li, C. Feng, F. Wu and R. Chen, *Adv. Funct. Mater.*, 2021, **31**, 2106676.
24 S. Ye, F. Liu, R. Xu, Y. Yao, X. Zhou, Y. Feng, X. Cheng and Y. Yu, *Small*, 2019, **15**, 1903725.
25 R. Pathak, K. Chen, A. Gurung, K. M. Reza, B. Bahrami, F. Wu, A. Chaudhary, N. Ghimire, B. Zhou and W. H. Zhang, *Adv. Energy Mater.*, 2019, **9**, 1901486.
26 L. Zeng, T. Zhou, X. Xu, F. Li, J. Shen, D. Zhang, J. Liu and M. Zhu, *Sci. China Mater.*, 2022, **65**, 337–348.
27 G. Huang, P. Guo, J. Wang, S. Chen, J. Liang, R. Tao, S. Tang, X. Zhang, S. Cheng and Y.-C. Cao, *Chem. Eng. J.*, 2020, **384**, 123313.
28 N. A. Sahalie, Z. T. Wondimkun, W.-N. Su, M. A. Weret, F. W. Fenta, G. B. Berhe, C.-J. Huang, Y.-C. Hsu and B. J. Hwang, *ACS Appl. Energy Mater.*, 2020, **3**, 7666–7679.
29 J. Sun, Y. Cheng, H. Zhang, X. Yan, Z. Sun, W. Ye, W. Li, M. Zhang, H. Gao and J. Han, *Nano Lett.*, 2022, **22**, 5874–5882.
30 X. Lu, J. Luo, E. Matios, Y. Zhang, H. Wang, X. Hu, C. Wang, H. Wang, J. Wang and W. Li, *Nano Energy*, 2020, **69**, 104446.
31 F. Liu, Z. Jin, Z. Hu, Z. Zhang, W. Liu and Y. Yu, *Chem. – Asian J.*, 2020, **15**, 1057–1066.
32 J. Sun, B. Li, C. Jin, L. Peng, D. Dai, J. Hu, C. Yang, C. Lu and R. Yang, *J. Power Sources*, 2021, **484**, 229253.
33 J. Zhang, Q. Li, Y. Zeng, Z. Tang, D. Sun, D. Huang, Z. Peng, Y. Tang and H. Wang, *Chem. Eng. J.*, 2021, **426**, 131110.
34 T. Le, C. Yang, W. Lv, Q. Liang, X. Huang, F. Kang and Y. Yang, *Adv. Sci.*, 2021, **8**, 2101940.
35 F. Tang, R. Xia, D. Chen, Y. Yao, L. Liu, Y. Feng, X. Rui and Y. Yu, *J. Energy Chem.*, 2022, **74**, 1–7.
36 S. T. Oyakhire, W. Zhang, A. Shin, R. Xu, D. T. Boyle, Z. Yu, Y. Ye, Y. Yang, J. A. Raiford and W. Huang, *Nat. Commun.*, 2022, **13**, 1–12.
37 B. Yu, T. Tao, S. Mateti, S. Lu and Y. Chen, *Adv. Funct. Mater.*, 2018, **28**, 1803023.
38 Z. Wang, L. Zhou and X. W. Lou, *Adv. Mater.*, 2012, **24**, 1903–1911.
39 L. Luo, J. Li, H. Yaghoobnejad Asl and A. Manthiram, *Adv. Mater.*, 2019, **31**, 1904537.
40 T. Zhang, H. Lu, J. Yang, Z. Xu, J. Wang, S.-I. Hirano, Y. Guo and C. Liang, *ACS Nano*, 2020, **14**, 5618–5627.
41 M. Lei, J.-G. Wang, L. Ren, D. Nan, C. Shen, K. Xie and X. Liu, *ACS Appl. Mater. Interfaces*, 2019, **11**, 30992–30998.
42 J. Zhu, J. Chen, Y. Luo, S. Sun, L. Qin, H. Xu, P. Zhang, W. Zhang, W. Tian and Z. Sun, *Energy Storage Mater.*, 2019, **23**, 539–546.

43 K. Lin, X. Qin, M. Liu, X. Xu, G. Liang, J. Wu, F. Kang, G. Chen and B. Li, *Adv. Funct. Mater.*, 2019, **29**, 1903229.
44 J. He and A. Manthiram, *Adv. Energy Mater.*, 2020, **10**, 1903241.
45 Q. Dong, B. Hong, H. Fan, H. Jiang, K. Zhang and Y. Lai, *ACS Appl. Mater. Interfaces*, 2019, **12**, 627–636.
46 D. Tang, L. Yuan, Y. Liao, W. Jin, J. Chen, Z. Cheng, X. Li, B. He, Z. Li and Y. Huang, *Sci. China Mater.*, 2022, **69**, 2385–2392.
47 J. Xiao, N. Xiao, C. Liu, H. Li, X. Pan, X. Zhang, J. Bai, Z. Guo, X. Ma and J. Qiu, *Small*, 2020, **16**, 2003827.
48 M. Liang, H. Xie, E. Liu, C. Shi, C. He and N. Zhao, *Carbon*, 2022, **196**, 795–806.
49 H. Yuan, J. Nai, H. Tian, Z. Ju, W. Zhang, Y. Liu, X. Tao and X. W. Lou, *Sci. Adv.*, 2020, **6**, eaaz3112.
50 F. Li, Y.-H. Tan, Y.-C. Yin, T.-W. Zhang, L.-L. Lu, Y.-H. Song, T. Tian, B. Shen, Z.-X. Zhu and H.-B. Yao, *Chem. Sci.*, 2019, **10**, 9735–9739.
51 W. Hou, S. Li, J. Liang, B. Yuan and R. Hu, *Electrochim. Acta*, 2022, **402**, 139561.
52 L. Zhao, Z. Hu, Z. Huang, Y. Tao, W. H. Lai, A. Zhao, Q. Liu, J. Peng, Y. Lei and Y. X. Wang, *Adv. Energy Mater.*, 2022, **12**, 2200990.
53 S. Q. Li, L. Zhang, T. T. Liu, Y. W. Zhang, C. Guo, Y. Wang and F. H. Du, *Adv. Mater.*, 2022, **24**, 2201801.
54 X. Zhou, F. Liu, Y. Wang, Y. Yao, Y. Shao, X. Rui, F. Wu and Y. Yu, *Adv. Energy Mater.*, 2022, **12**, 2202323.
55 C. Sun, A. Lin, W. Li, J. Jin, Y. Sun, J. Yang and Z. Wen, *Adv. Energy Mater.*, 2020, **10**, 1902989.
56 P. Xu, X. Hu, X. Liu, X. Lin, X. Fan, X. Cui, C. Sun, Q. Wu, X. Lian and R. Yuan, *Energy Storage Mater.*, 2021, **38**, 190–199.
57 H. Jiang, Y. Zhou, H. Zhu, F. Qin, Z. Han, M. Bai, J. Yang, J. Li, B. Hong and Y. Lai, *Chem. Eng. J.*, 2022, **428**, 132648.
58 C. Fu, S. Lin, C. Zhao, J. Wang, L. Wang, J. L. Bao, Y. Wang and T. Liu, *Energy Storage Mater.*, 2022, **45**, 1109–1119.
59 Y. Liu, M. Bai, D. Du, X. Tang, H. Wang, M. Zhang, T. Zhao, F. Liu, Z. Wang and Y. Ma, *Energy Environ. Mater.*, 2022, **6**, e12350.
60 X. Zhang, S. Jin, M. H. Seo, C. Shang, G. Zhou, X. Wang and G. Li, *Nano Energy*, 2022, **93**, 106905.
61 X. Wang, Z. Na, D. Yin, C. Wang, Y. Wu, G. Huang and L. Wang, *ACS Nano*, 2018, **12**, 12238–12246.
62 L. Que and W. Chen, *J. Power Sources*, 2023, **557**, 232536.
63 C. Yuan, L. Yin, P. Du, Y. Yu, K. Zhang, X. Ren, X. Zhan and S. Gao, *Chem. Eng. J.*, 2022, **442**, 136231.
64 M. Z. Mayers, J. W. Kaminski and T. F. Miller III, *J. Phys. Chem. C*, 2012, **116**, 26214–26221.
65 G. Milazzo, S. Caroli and R. D. Braun, *J. Electrochem. Soc.*, 1978, **125**, 261C.
66 H. Zhang, X. Liao, Y. Guan, Y. Xiang, M. Li, W. Zhang, X. Zhu, H. Ming, L. Lu and J. Qiu, *Nat. Commun.*, 2018, **9**, 1–11.
67 M. Wang, W. Wang, Y. Meng, Y. Xu, J. Sun, Y. Yuan, M. Chuai, N. Chen, X. Zheng and R. Luo, *Energy Storage Mater.*, 2023, **56**, 424–431.
68 J. Chen, Y. Wang, S. Li, H. Chen, X. Qiao, J. Zhao, Y. Ma and H. N. Alshareef, *Adv. Sci.*, 2023, **10**, 2205695.
69 S. Abdul Ahad, T. E. Adegoke, K. M. Ryan and H. Geaney, *Small*, 2023, DOI: **10.1002/smll.202207902**.
70 S. Pyo, S. Ryu, Y. J. Gong, J. Cho, H. Yun, H. Kim, J. Lee, B. Min, Y. Choi and J. Yoo, *Adv. Energy Mater.*, 2023, **13**, 2203573.
71 Y. K. Lee, K. Y. Cho, S. Lee, J. Choi, G. Lee, H. I. Joh, K. Eom and S. Lee, *Adv. Energy Mater.*, 2023, **13**, 2203770.
72 P. Xue, C. Sun, H. Li, J. Liang and C. Lai, *Adv. Sci.*, 2019, **6**, 1900943.
73 A. Mohammadi, L. Monconduit, L. Stievano and R. Younesi, *J. Electrochem. Soc.*, 2022, 070509.
74 A. Bard, *Standard potentials in aqueous solution*, Routledge, 2017.
75 W. Wu, H. Feng and K. Wu, *Standard electrode potential Data manual*, Sciences Press, 1991.
76 R. Huston and J. N. Butler, *J. Phys. Chem. C*, 1968, **72**, 4263–4264.
77 J. Desreumaux, M. Calais, R. Adriano, S. Trambaud, C. Kappenstein and M. Nguefack, *Eur. J. Inorg. Chem.*, 2000, 2031–2045.
78 W. M. Haynes, D. R. Lide and T. J. Bruno, *CRC handbook of chemistry and physics*, CRC Press, 2016.
79 J. Dean, *Lange's Handbook of Chemistry, WEI Junfa Trans*, Science Press, Beijing, 2003.
80 A. J. Dill, L. M. Itzkowitz and O. Popovych, *J. Phys. Chem. C*, 1968, **72**, 4580–4586.
81 F. Wu, M. Wang, Y. Su and S. Chen, *J. Power Sources*, 2009, **189**, 743–747.
82 H. Wang, E. Matios, J. Luo and W. Li, *Chem. Soc. Rev.*, 2020, **49**, 3783–3805.
83 A. R. Rashid, A. G. Abid, S. Manzoor, A. Mera, T. I. Al-Muhimeed, A. A. AlObaid, S. N. Shah, M. N. Ashiq, M. Imran and M. Najam-Ul-Haq, *Ceram. Int.*, 2021, **47**, 28338–28347.
84 J. Li, H. Wei, F. Hu, Z. Xie, J. Hei, Y. Kong, X. Yin, N. Wang and H. Wei, *Int. J. Hydrogen Energy*, 2022, **47**, 32594–32606.
85 J. Zhang, Y. Li, L. Zhu, X. Wang and J. Tu, *Energy Storage Mater.*, 2021, **41**, 606–613.
86 M. Wang, N. Chen, Z. Zhu, Y. Meng, C. Shen, X. Zheng, D. Liang and W. Chen, *Small*, 2021, **17**, 2103921.
87 Y. Yao, Z. Chen, R. Yu, Q. Chen, J. Zhu, X. Hong, L. Zhou, J. Wu and L. Mai, *ACS Appl. Mater. Interfaces*, 2020, **12**, 40648–40654.
88 L. Wang, L. Zhang, Q. Wang, W. Li, B. Wu, W. Jia, Y. Wang, J. Li and H. Li, *Energy Storage Mater.*, 2018, **10**, 16–23.
89 H. Huang, Y. Wang, M. Li, H. Yang, Z. Chen, Y. Jiang, S. Ye, Y. Yang, S. He and H. Pan, *Adv. Mater.*, 2023, DOI: **10.1002/adma.202210826**.
90 L. Chen, G. Chen, W. Tang, H. Wang, F. Chen, X. Liu and R. Ma, *Mater. Today Energy*, 2020, **18**, 100520.
91 F. Liu, Z. Jin, Z. Hu, Z. Zhang, W. Liu and Y. Yu, *Chem. – Asian J.*, 2020, **15**, 1057–1066.
92 M. Mayo, K. J. Griffith, C. J. Pickard and A. J. Morris, *Chem. Mater.*, 2016, **28**, 2011–2021.

93 J. Zhu, D. Cai, J. Li, X. Wang, X. Xia, C. Gu and J. Tu, *Energy Storage Mater.*, 2022, **49**, 546–554.
94 D. Lee, S. Sun, J. Kwon, H. Park, M. Jang, E. Park, B. Son, Y. Jung, T. Song and U. Paik, *Adv. Mater.*, 2020, **32**, 1905573.
95 H. Park, J. Kwon, T. Song and U. Paik, *J. Power Sources*, 2020, **477**, 228776.
96 X. Zhang, F. Ma, K. Srinivas, B. Yu, X. Chen, B. Wang, X. Wang, D. Liu, Z. Zhang and J. He, *Energy Storage Mater.*, 2022, **45**, 656–666.
97 H. Cheng, D. Li, B. Xu, Y. Wei, H. Wang, B. Jiang, X. Liu, H. Xu and Y. Huang, *Energy Storage Mater.*, 2022, **53**, 305–314.
98 N. Pavlushkin and L. Egorova, *Atlas of thermoanalytical curves*, 1979.
99 J. Wang, N. Miao, P. Chartrand and I.-H. Jung, *J. Chem. Thermodyn.*, 2013, **66**, 22–33.
100 R. Jain, Y. Yuan, Y. Singh, S. Basu, D. Wang, A. Yang, X. Wang, M. Rong, H. J. Lee and D. Frey, *Adv. Energy Mater.*, 2021, **11**, 2003248.
101 H. Ye, Z. J. Zheng, H. R. Yao, S. C. Liu, T. T. Zuo, X. W. Wu, Y. X. Yin, N. W. Li, J. J. Gu and F. F. Cao, *Angew. Chem., Int. Ed.*, 2019, **58**, 1094–1099.
102 J. Wu, X. Chen, W. Fan, X. Li, Y.-W. Mai and Y. Chen, *Energy Storage Mater.*, 2022, **48**, 223–243.
103 S. Zhang, G. Wang, J. Jin, L. Zhang, Z. Wen and J. Yang, *Nano Energy*, 2017, **36**, 186–196.
104 H. Liu, X.-B. Cheng, J.-Q. Huang, S. Kaskel, S. Chou, H. S. Park and Q. Zhang, *ACS Mater. Lett.*, 2019, **1**, 217–229.